

# Tracking Attosecond Electronic Coherences using Phase-Manipulated Extreme Ultraviolet Pulses

Andreas Wituschek<sup>1\*</sup>, Lukas Bruder<sup>1,2\*</sup>, Enrico Allaria<sup>3</sup>, Ulrich Bangert<sup>1</sup>, Marcel Binz<sup>1</sup>, Carlo Callegari<sup>3</sup>, Giulio Cerullo<sup>4</sup>, Paolo Cincquegrana<sup>3</sup>, Luca Gianessi<sup>3</sup>, Miltcho Danailov<sup>3</sup>, Alexander Demidovich<sup>3</sup>, Michele Di Fraia<sup>3</sup>, Marcel Drabbels<sup>5</sup>, Raimund Feifel<sup>6</sup>, Tim Laarmann<sup>7,8</sup>, Rupert Michiels<sup>1</sup>, Najmeh Sadat Mirian<sup>3</sup>, Marcel Mudrich<sup>9</sup>, Ivaylo Nikolov<sup>3</sup>, Finn H. O'Shea<sup>3</sup>, Giuseppe Penco<sup>3</sup>, Paolo Piseri<sup>10</sup>, Oksana Plekan<sup>3</sup>, Kevin Charles Prince<sup>3</sup>, Andreas Przystawik<sup>7</sup>, Primož Rebernik Ribič<sup>3</sup>, Giuseppe Sansone<sup>1</sup>, Paolo Sigalotti<sup>3</sup>, Simone Spampinati<sup>3</sup>, Carlo Spezzani<sup>3</sup>, Richard James Squibb<sup>6</sup>, Stefano Stranges<sup>11</sup>, Daniel Uhl<sup>1</sup> & Frank Stienkemeier<sup>1,12</sup>

<sup>1</sup>Institute of Physics, University of Freiburg, Freiburg, Germany

<sup>2</sup>Chemical Physics, Lund University, Lund, Sweden.

<sup>3</sup>Elettra-Sincrotrone Trieste S.C.p.A., Trieste, Italy

<sup>4</sup>IFN-CNR and Dipartimento di Fisica, Politecnico di Milano, Milan, Italy

<sup>5</sup>Laboratory of Molecular Nanodynamics, Ecole Polytechnique Fédérale Lausanne, Lausanne, Switzerland

<sup>6</sup>Department of Physics, University of Gothenburg, Gothenburg, Sweden

<sup>7</sup>Deutsches Elektronen-Synchrotron DESY, Hamburg, Germany

<sup>8</sup>The Hamburg Centre for Ultrafast Imaging CUI, Hamburg, Germany.

<sup>9</sup>Department of Physics and Astronomy, Aarhus University, Aarhus, Denmark

<sup>10</sup>Università degli Studi di Milano, Milan, Italy

<sup>11</sup>University of Rome "La Sapienza", Rome, Italy

<sup>12</sup>Freiburg Institute of Advanced Studies, University of Freiburg, Freiburg, Germany

\*Correspondence to: andreas.wituschek@physik.uni-freiburg.de, lukas.bruder@physik.uni-freiburg.de

June 17, 2019

**The recent development of novel extreme ultraviolet (XUV) coherent light sources bears great potential for a better understanding of the structure and dynamics of matter<sup>1,2</sup>. Promising routes are advanced coherent control and nonlinear spectroscopy schemes in the XUV energy range, yielding unprecedented spatial and temporal resolution<sup>3,4</sup>. However, their implementation has been hampered by the experimental challenge of generating XUV pulse sequences with precisely controlled timing and phase properties. In particular, direct control and manipulation of the phase of individual pulses within a XUV pulse sequence opens exciting new possibilities for coherent control and multidimensional spectroscopy schemes<sup>4</sup>,**

**but has not been accomplished. Here, we overcome these constraints in a highly time-stabilized and phase-modulated XUV-pump, XUV-probe experiment which directly probes the evolution and dephasing of an inner subshell electronic coherence. This new approach, avoiding any XUV optics for direct pulse manipulation, opens up extensive applications of advanced nonlinear optics and spectroscopy at XUV wavelengths.**

Coherent phenomena are an intriguing aspect of the quantum world. Their dynamics reveal rich information on a quantum system including ultrafast decay mechanisms and couplings to its environment. Prominent examples are vibrational wave packet (WP) oscillations, directly reflecting the nuclear motion of a molecule<sup>5</sup>, electronic Rydberg WPs describing the classical orbit of an electron<sup>6</sup> or extremely long-lived spin WPs in diamond vacancies, serving as qubit storage devices in quantum communication applications<sup>7</sup>.

To probe coherent dynamics in real time, specialized ultrafast methods are necessary which rely on interferometric measurements, mapping the oscillatory phase evolution of excited coherences<sup>8</sup>. This is most challenging for the electronic degrees of freedom where oscillation periods scale inversely with excitation energy and thus require extremely high timing stability in the atto- to zeptosecond range. Yet, to capture the full dynamical picture of a system, it is essential to track the evolution of all degrees of freedom including electronic coherences<sup>9,10</sup>.

The extension of coherent time-resolved spectroscopy to XUV photon energies is highly desirable as it offers unprecedented site-specificity by accessing localized inner-shell states and opens the door to attosecond time resolution<sup>2</sup>. However, these experiments are extremely challenging due to the required ultra-high phase stability and the lack of phase matching/cycling schemes necessary to isolate subtle coherence signals. For these reasons, a real-time study of the evolution of an XUV

electronic coherence has not been reported and only few examples of quantum beat and vibrational WP studies have been demonstrated, so far<sup>11,12</sup>.

Coherent control in the XUV spectral range is a second field of high interest which likewise relies on the preparation and probing of coherent states of matter. In a bichromatic approach, coherent control was achieved by controlling the relative delay between two XUV pulses<sup>13</sup>. Another, more general approach, relies on phase manipulation of the XUV pulses. Pulse shaping technology, only available in the infrared to ultraviolet spectral range, has enabled advanced control schemes, with applications in nonlinear optics and the steering of chemical reactions<sup>14</sup>. In the XUV, phase manipulation has been indirectly shown by varying the chirp<sup>15</sup> or polarization<sup>16</sup> of the driving field. However, direct and independent manipulation of the relative phase and delay of XUV pulses in a pulse sequence has not been accomplished so far.

In this work, we implement a phase-modulation technique for XUV pulse sequences which facilitates both flexible coherent control schemes and advanced coherent nonlinear spectroscopy techniques. To this end, phase-locked XUV pulse pairs with full control over delay and relative phase were prepared at the FERMI free-electron laser<sup>17</sup> (FEL) using twin seeding<sup>18</sup> with phase-manipulated seed pulse pairs (Fig. 1). The intense phase-locked ultraviolet (UV) seed pulse pairs are created with a highly stable optical interferometer based on a monolithic design<sup>19</sup>, and used to seed the FEL process by means of the high gain harmonic generation (HGHG) scheme. This leads to the emission of fully coherent XUV pulse pairs at a specific harmonic of the seed wavelength<sup>20</sup>.

Previous experiments indicated the possibility of XUV phase manipulation through the seed pulse properties<sup>15,18</sup>. In the current work, we explicitly exploit the phase relation between seed and XUV pulses to achieve high precision active phase control of XUV pulse pairs while avoiding the challenge of phase shaping at XUV wavelengths. For this purpose, two phase-locked acousto-

optical modulators (AOMs) control the relative phase  $\phi_{21} = \phi_2 - \phi_1$  of the seed pulses (Fig. 1). Upon HHG, the imprinted phase transfers to a well-defined phase shift of  $n\phi_{21}$  for the XUV pulses at the  $n^{\text{th}}$  harmonic, enabling flexible phase manipulation (Fig. 2a). The applied twin-seeding concept allows for even higher pump-probe timing control than advanced XUV split-and-delay units<sup>21</sup> and is not restricted to bichromatic pump-probe schemes<sup>13</sup>.

The XUV phase control is demonstrated by manipulating the phase of XUV Ramsey-type interference fringes for photon energies up to 47.5 eV (Fig. 2b, c). The high quality of timing and phase control is directly reflected in the interferograms. The highly stable seed laser interferogram indicates that the phase stability is not limited by our interferometric setup but by the phase jitter picked up during the HHG process. Here, timing jitter between seed pulses and the electron bunch ( $\approx 100$  fs rms) leads to phase jitter of the produced XUV pulses due to the residual longitudinal energy chirp of the electron bunch<sup>18</sup>. However, this noise source can be minimized using echo-enabled harmonic generation recently demonstrated in the XUV to soft X-ray regime at FERMI<sup>22</sup>.

We note that in comparison to established pulse shaping technologies our approach can handle the required high seed pulse energies ( $> 10$   $\mu\text{J}$ ) and provides a high purity, artifact-free phase manipulation. This is crucial for the application in strongly nonlinear processes such as high harmonic generation, where any phase shaping distortion is amplified by the nonlinear process. Furthermore, our concept allows for the independent control of both timing and phase properties of the XUV pulses, which has so far not been achieved. Combined with multiple-pulse seeding, many pulse shaping and nonlinear spectroscopy applications can be realized now at XUV wavelengths.

Examples of applications of this concept are advanced coherent spectroscopy schemes based on phase cycling concepts<sup>23</sup>. In the IR to UV spectral range, phase cycling has drastically improved

the detection sensitivity and paved the way for a plethora of nonlinear spectroscopy schemes<sup>24,25</sup>. In the XUV, these experiments are extremely challenging, as they involve sequences of multiple phase-locked XUV pulses with independently controllable timing and phase parameters. Here, we demonstrate such an experiment by tracking the temporal evolution of attosecond electronic coherences with phase-modulated XUV-pulse sequences.

The model system examined is the  $1s^2 \rightarrow 1s4p$  transition in helium (Fig. 3a). The first XUV pulse creates a coherent superposition of ground and excited state (electronic WP), denoted  $|\psi(t)\rangle$ . The second XUV pulse delayed by  $\tau$  projects this WP onto a stationary population state, which is probed by selective ionization of the  $1s4p$  state with a NIR pulse, yielding the signal  $S \propto \langle \psi(\tau) | 1s4p \rangle = A(\tau)e^{i\phi(\tau)}$ , where  $A(\tau)$  denotes the amplitude and  $\phi(\tau)$  the phase evolution of the WP. According to the  $1s^2 \rightarrow 1s4p$  transition energy  $E = 23.74$  eV, the signal would oscillate with a period of  $h/E = 174$  as, requiring an extremely high pump-probe timing stability of  $\delta\tau < 20$  as (corresponding to an optical path stability of  $\delta_{OP} < 6$  nm) for adequate sampling.

Here, we apply a specialized phase cycling scheme to solve this problem. By combining phase modulation of both XUV pulses with phase-synchronous lock-in detection, we are able to downshift the signal oscillation period by a factor of  $> 50$  (rotating frame detection<sup>26</sup>) and remove most of the phase jitter from the signal while improving the overall sensitivity through efficient lock-in amplification (details in Methods section). Fig. 3b shows the respective time domain interferogram recorded for the helium excitation, exhibiting clean periodic oscillations of the induced attosecond electronic WP in excellent agreement with theory (Fig. 3c). The good data quality is remarkable considering the applied low FEL energy ( $\leq 30$  nJ) and the probed low atom density ( $\approx 10^{14} \text{ cm}^{-3}$ ), showing the high signal-to-noise performance and sensitivity of the method, even with the challenging XUV wavelength conditions.

The signal quality furthermore allows for direct Fourier analysis to gain spectral information (Fig 3d), yielding a frequency spectrum with a signal to noise ratio of 9. Careful preparation of the electron bunch combined with the reduced acquisition times due to rotating frame sampling allowed us to monitor the WP oscillations up to 700 fs, leading to a high spectral resolution in the Fourier domain ( $\sigma = 6$  meV for a gaussian peak). This is slightly better than what is achieved with XUV spectrometers in transient absorption experiments<sup>27,28</sup>. In addition, the Fourier transform approach combines spectral resolution with highly selective detection types, here demonstrated for mass-resolved photoion and energy-gated photoelectron detection. In combination with phase-cycling, this allowed for highly efficient suppression of background contributions (background/signal ratio = 200).

At short delays where both seed pulses overlap temporally (<150 fs), twin-pulse seeding is expected to break down due to the non-linear response of the density modulation initiating the FEL process to optical interference effects, causing shot-to-shot amplitude modulation of the FEL radiation. This explains the amplitude drop of our data at <150 fs. Interestingly, we can still observe a clear oscillation and a stable signal phase (not shown), indicating that information be may also gained from this region.

The helium study served as a model for an unperturbed quantum system exhibiting long-lived electronic coherences and negligible dephasing. In argon, we investigate a different situation for the  $3s^23p^6 \rightarrow 3s^13p^66p^1$  transition. The 6p valence orbital couples to the  $Ar^+$  continuum via configuration interaction (Fig. 4a), opening up an autoionizing pathway that introduces significant dephasing. Phase shifts between the quantum pathways for direct ionization from the ground state and autoionization via the resonance lead to characteristic Fano line shapes<sup>29</sup>. Fano resonances in argon have been observed in the frequency domain with synchrotron radiation<sup>30</sup> and in the time

domain with attosecond transient absorption<sup>31</sup>. Recently, with the help of the phase information imprinted on the Fano line shape, the reconstruction of a two-electron wave packet was achieved<sup>27</sup>. However, so far, the full dynamics including electronic coherences were not accessible and the phase information was inferred from theoretical assumptions.

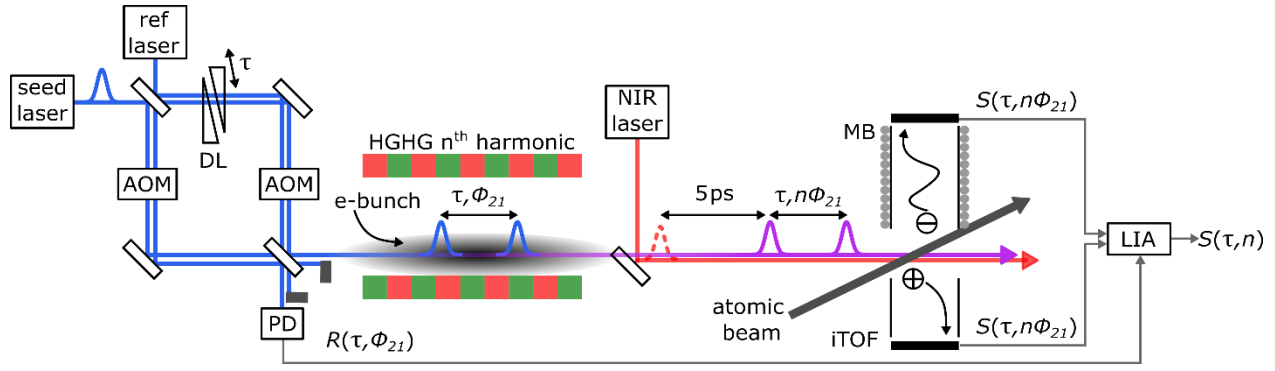
We have overcome this limitation by measuring the electronic dephasing of a Fano resonance in the time domain. As an advantage, our phase-sensitive lock-in detection directly provides  $A(\tau)$  and  $\phi(\tau)$  which allows for the full reconstruction of the probed quantum state (up to an arbitrary phase offset). Note, that unlike in other phase retrieval concepts<sup>27,32</sup>,  $\phi(\tau)$  is directly obtained without the need of an iterative algorithm or theoretical considerations. Unfortunately, technical problems during the beamtime caused a faulty delay calibration for the argon measurement, imposing an uncertainty of 1.1 rad on the absolute phase value. However, for future studies the absolute phase uncertainty is expected to be much smaller.

Figure 4b shows the signal amplitude and phase evolution in the time domain. Note that here the third pulse for ionization is not necessary. A Fourier transform of the complex-valued signal  $S(\tau) = A(\tau)e^{i\phi(\tau)}$  yields the respective absorption and dispersion curves of the process in which the typical Fano line shape is recovered (Fig. 4c). The line shape and the spectral width are in good agreement with synchrotron measurements<sup>30</sup>, indicating that we obtain the correct time scale and phase of the decaying coherence.

To the best of our knowledge, this is the first direct observation of the dephasing of an inner subshell - valence shell coherence. While electronic dephasing is studied in many examples in the visible, in the XUV range it may provide selective information about the coupling of a specific site to the environment or real-time information about intra- and inter-particle decay mechanisms.

In conclusion, we introduced a highly sensitive phase-cycling based coherent spectroscopy technique at XUV wavelengths and tracked the attosecond time evolution of electronic WPs with high phase precision. Scaling photon energies with novel FEL seeding concepts<sup>22</sup> will allow localized core states to be addressed. In addition, the unprecedented sensitivity of our method provides ideal conditions for applications with tabletop high harmonic sources, where attosecond experiments will greatly benefit from the improved stability and sensitivity. These properties combined with the established phase cycling concept, introduce a new, versatile XUV spectroscopy toolbox for the wide range application of specialized nonlinear spectroscopy schemes, so far only accessible at visible wavelengths. Specifically designed detection protocols to address fundamental problems of ultrafast non-adiabatic dynamics<sup>33</sup>, many-body phenomena<sup>4</sup> or the control of chemical reactions along complex energy landscapes may now be realized in the XUV regime.





**Figure 1. Experimental scheme.** Intense twin-seed pulses are generated in an ultra-stable monolithic interferometer. The pulse delay  $\tau$  is set by a wedge-based delay line (DL) and phase-locked acousto-optical modulators (AOMs) control the relative phase  $\phi_{21}$  of the seed pulses. The time and phase controlled pulse pairs seed the high-gain harmonic generation (HGHG) process in the FEL, resulting in coherent XUV pulse pairs with precisely controlled timing and relative phase. The XUV pulse pair tracks the real time evolution of electronic coherences induced in an atomic beam sample. Detection is done via photoionization with a third pulse from a near infrared (NIR) laser, and photoproducts (electrons/ions) are detected in coincidence with a magnetic bottle (MB) and ion time-of-flight spectrometer (iTOF). A continuous-wave reference laser is used to trace the phase evolution and jitter in the interferometer, recorded with a photodiode (PD). This signal is used for rotating frame sampling and phase-sensitive detection of the mass/energy-gated ion/electron yields with a lock-in amplifier (LIA).

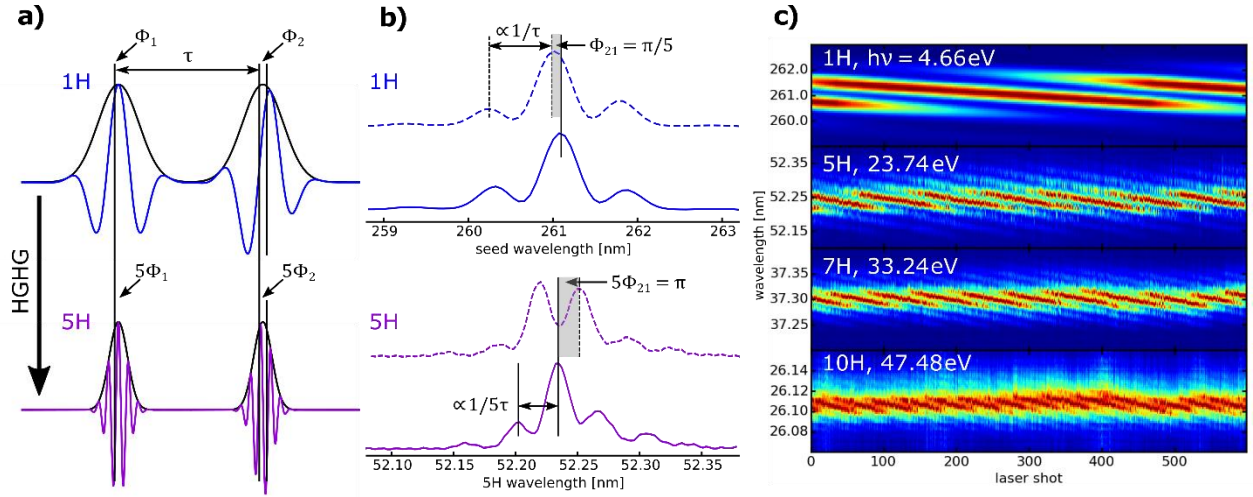


**Figure 2. XUV phase manipulation.** (a) Timing and phase control of the XUV pulse pair (violet) by manipulation of the seed pulse (blue) parameters. In this scheme, manipulation of pulse delay  $\tau$  and phase difference  $\phi_{21} = \phi_2 - \phi_1$  are decoupled. (b) Ramsey-type interference fringes for fixed delay  $\tau = 250$  fs and two different phase values  $\phi_{21}$  recorded for the seed (blue) and its 5<sup>th</sup> harmonic (violet), respectively. The fringe spacing is inversely proportional to the pulse delay  $\sim 1/\tau$ , while the fringe phase is directly proportional to the phase difference  $\sim \phi_{21}$ . (c) Recorded Ramsey fringes of the seed (1H) and different harmonic FEL pulses (5H-10H). Here,  $\phi_{21}$  was incremented by 15 mrad steps in-between each laser shot leading to a quasi-continuous phase sweep. Full phase rotations of several periods of  $2\pi$  are demonstrated without modification of the relative pulse delays. At the 10<sup>th</sup> harmonic, the spectrometer resolution is on the order of the fringe spacing, compromising the data quality slightly. All Ramsey-type fringes correspond to normalized single-shot events with no additional data processing applied.

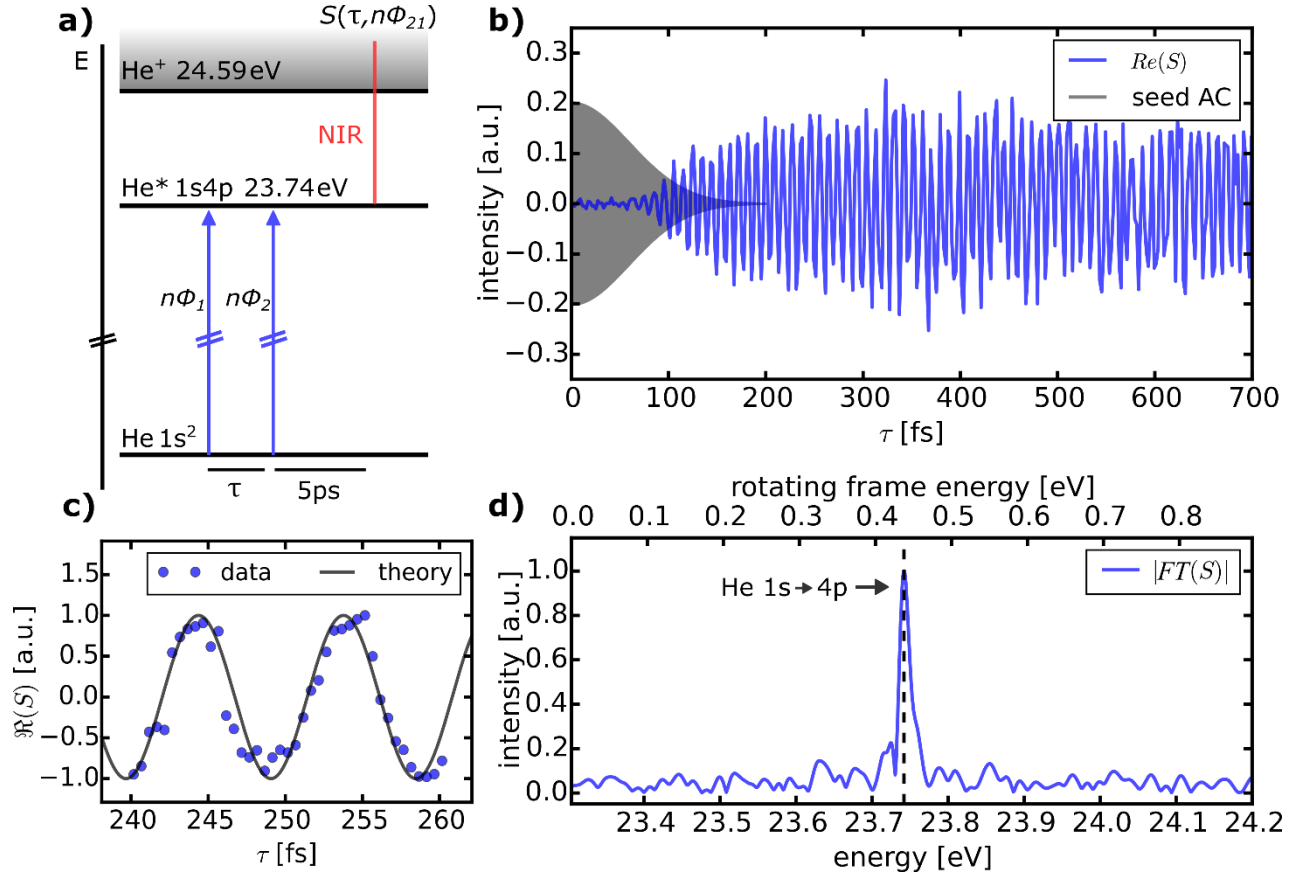


**Figure 3. XUV electronic coherence in helium.** (a) Energy scheme of helium with relevant levels and interaction pathways. (b) Real part of the downshifted WP signal, with the delay incremented in 2 fs steps. Temporal overlap region of seed pulses is indicated (grey area). (c) Comparison with theory, here the delay increment is 500 as. (d) Fourier transform (absolute value) of the signal, showing the He  $1s \rightarrow 4p$  resonance. The upper energy scale corresponds to frequency spectrum of the downshifted data acquired in the rotating frame, the lower energy scale shows corresponding absolute energy values. Each data point corresponds to only 240 FEL shots, no additional filtering or post processing has been applied.

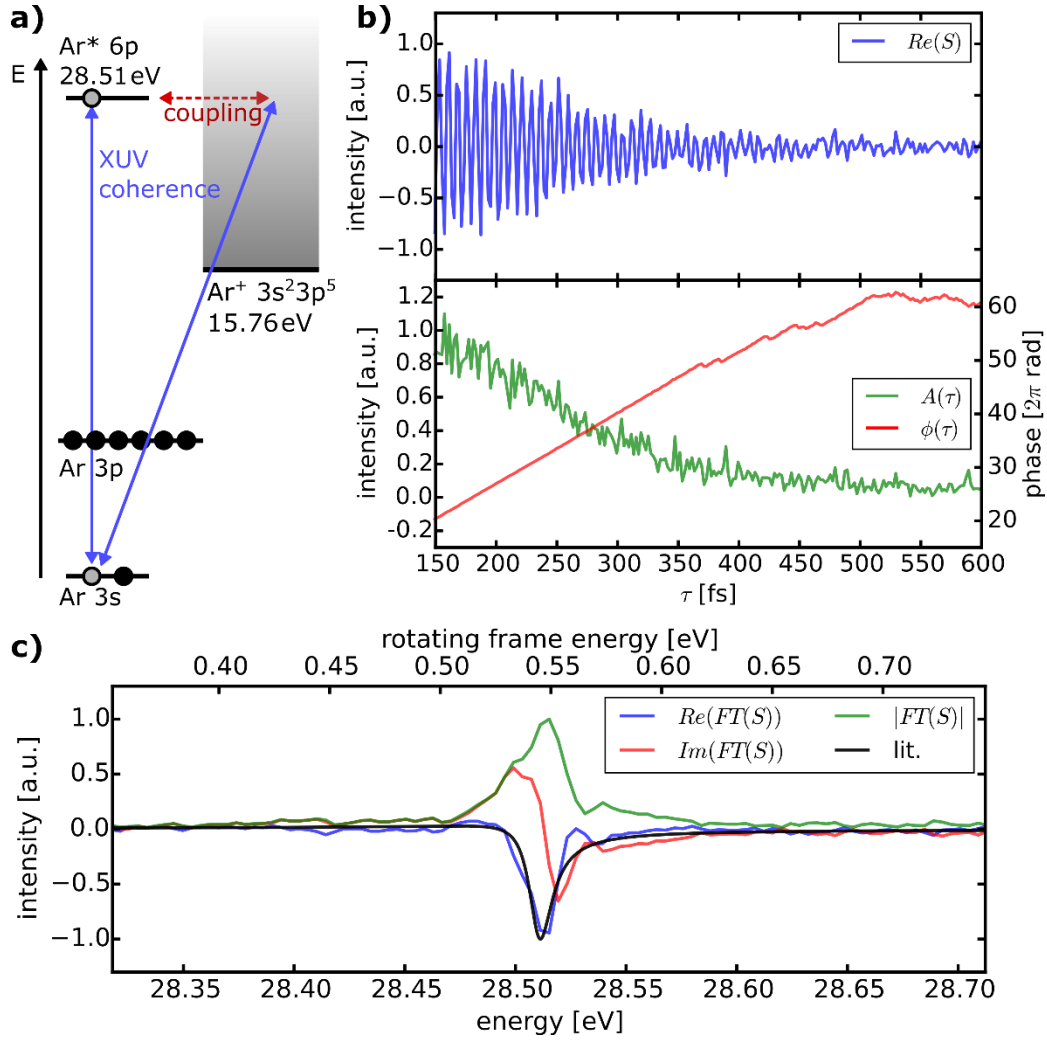


**Figure 4. Phase-resolved real-time dephasing of a Fano resonance in argon.** (a) Excitation scheme for preparation and probing of the Ar 3s-6p inner subshell-valence coherence. (b) Decay of the 3s-6p coherence in the time domain, with real part of the complex signal  $S = A(\tau)e^{i\phi(\tau)}$  (blue) and its decomposition into amplitude  $A(\tau)$  (green) and phase  $\phi(\tau)$  (red). (c) Linear susceptibility of the process obtained from Fourier transform of the signal: Absorption (real part, blue) and dispersion (imaginary part, red) curve compared to the Fano lineshape from Ref. 28 (black). For comparison, without phase-sensitive detection, only the absolute value of the signal Fourier transform (green) would be accessible which cannot recover the Fano lineshape, since the phase information of involved quantum pathways is missing.

## Methods

### Phase-modulated coherent time domain XUV spectroscopy:

A single seed laser pulse ( $\lambda \approx 261$  nm,  $\Delta t = 100$  fs fwhm) is split in a Mach-Zehnder interferometer (MZI), creating a phase-locked pulse pair with controllable delay  $\tau$ . Two acousto-optical modulators (AOMs) are driven with continuous wave radio frequencies (RF) in phase locked mode. Each driving frequency can be controlled with 0.12 Hz frequency and 380  $\mu$ rad phase resolution. The relative phase  $\phi_{21}$  between the pulses is controlled by manipulating frequency and phase of the driving fields. In the modulator section of the FEL the twin-seed pulses interact with a relativistic electron bunch. Thereby amplitude and phase of the twin-seed pulse are imprinted on the longitudinal phase space of the electron bunch. This transfers to an electron density modulation in a dispersive chicane, finally leading to the emission of an XUV pulse pair at a specific harmonic of the seed wavelength in subsequent undulators.

We use the phase modulation technique developed by Marcus and coworkers<sup>34</sup>, to perform phase-modulated coherent time domain XUV spectroscopy. We increment  $\phi_{21}$  on a shot-to-shot basis, leading to a quasi-continuous modulation of  $\phi_{21}$  at a frequency of  $\Omega \approx 3$  Hz. Via the HGHG process, the relative phase of the XUV pulses transfers to  $n\phi_{21}$ , leading to a phase modulation at a frequency of  $n\Omega$ . The XUV pulse pair creates an electronic WP  $|\psi\rangle$  between the ground and the excited state  $|g\rangle$  and  $|e\rangle$ , respectively. We monitor the temporal evolution of the WP by ionization out of the excited state. In the case of helium this was realized with an additional synchronized NIR laser, while argon ions were obtained by autoionization. The evolution of the WP gives rise to delay dependent oscillations in the ion yield  $S(\tau) \propto A(\tau)\cos(\omega_{eg}\tau + \phi_0)$ . Here  $\omega_{eg}$  is the transition frequency from the ground to the excited state, and  $\phi_0$  is a phase shift determined by the parameters of the WP. The phase modulation imparts an additional real time modulation on the ion

yield:  $S(\tau, t) \propto A(\tau) \cos(\omega_{eg}\tau - n\Omega t)$ . Simultaneously, we collinearly trace the MZI with a narrowband 266 nm continuous wave laser, which undergoes the same phase-modulation and records all jitter inside the MZI, serving as a reference for lock-in detection:  $R(\tau, t) \propto \cos(\omega_{ref}\tau - \Omega t)$ , where  $\omega_{ref}$  is the optical frequency of the reference laser. Referencing the lock-in amplifier to a harmonic of  $R$  (same harmonic as in the HGHG process) and demodulating  $S$  therewith yields the in-phase (real part) and in-quadrature components (imaginary party) of  $S$ , allowing for the reconstruction of the downshifted complex valued WP oscillations  $S(\tau) \propto A(\tau) \exp(i(\omega_{ng} - n\omega_{ref})\tau + i\phi_0)$ . Due to the rotating frame detection, the fast WP oscillations are downshifted by  $n$ -times the amount of the reference laser frequency. Furthermore, all phase jitter arising from the MZI cancels efficiently during the demodulation process. However, phase jitter picked up in the beam path after the MZI is not removed during the demodulation process as it is not imprinted in  $R$ . Spectral information is deduced by Fourier transforming the downshifted quantum oscillations  $\mathcal{F}(S(\tau))$ . Here the real and imaginary parts correspond to the absorptive and dispersive parts of the line shape, respectively<sup>34</sup>. More details of the optical seed laser phase modulation setup and the harmonic lock-in demodulation scheme can be found in Refs. 18 and 33, respectively.

### **FEL setup and sample preparation:**

We tuned the FEL photon energy to  $h\nu = 23.74$  eV for helium, and 28.51 eV for argon. The FEL pulse duration estimated from the spectral bandwidth was  $58 \pm 6$  fs, which is in good agreement with the predictions from literature<sup>35</sup>. The helium beam was generated by supersonic expansion through a pulsed nozzle, yielding a density of  $\approx 10^{14} \text{ cm}^{-3}$  in the interaction region. The argon beam was created by effusion through an aperture, yielding a much lower density of  $\approx 10^9 \text{ cm}^{-3}$ . In order to avoid saturation of the detection electronics and space charge effects the FEL energies were adjusted using metal filters, yielding  $\leq 30$  nJ and  $\approx 10$   $\mu$ J per pulse for the helium and the

argon study, respectively. The FEL repetition rate was 50 Hz. In order to provide similar parameters of the electron bunch for both seed pulses at all delays, the longitudinal beam properties should be as uniform as possible. This was achieved by reducing the compression of the electron bunch, yielding a sufficiently flat region along the bunch, allowing for a useful delay range of  $\approx 1$  ps. The XUV pulses were focused into the atomic beam to a diameter of 70  $\mu\text{m}$  FWHM.

## **Data availability**

The data that support the findings of this study are available from the corresponding author upon reasonable request.

## **Acknowledgements**

Funding by the Bundesministerium für Bildung und Forschung (BMBF, 05K16VFB), by the European Research Council (ERC) with the Advanced Grant “COCONIS” (694965) and by the Deutsche Forschungsgemeinschaft (DFG) IRTG CoCo (2079) is acknowledged.

## **Author contributions**

A.W., L.B. and F.S. conceived the experiment. A.W., L.B., P.C., A.D., M.D., I.N. and P.S. prepared the seed laser phase modulation setup. E.A., L.G., N.S.M., G.P., P.R.R., C.S., F.H.S. and S.Sp. prepared the FEL. A.W., C.C., M.D.F., R.M., O.P., R.J.S. and D.U. prepared the endstation. A.W., L.B., M.B., U.B., C.C., G.C., M.D., M.D.F., R.F., T.L., M.M., R.M., A.P., K.C.P., O.P., P.P., G.S., R.J.S., S.St., D.U., and F.S. performed the measurements. A.W. and L.B. wrote the manuscript with input from all other authors.

## **Competing interests**

The authors declare no competing financial interests.

## **References and Notes**

1. Kraus, P. M., Zürich, M., Cushing, S. K., Neumark, D. M. & Leone, S. R. The ultrafast X-ray spectroscopic revolution in chemical dynamics. *Nat. Rev. Chem.* **2**, 82 (2018).
2. Young, L. *et al.* Roadmap of ultrafast x-ray atomic and molecular physics. *J. Phys. B At. Mol. Opt. Phys.* **51**, 032003 (2018).
3. Ramasesha, K., Leone, S. R. & Neumark, D. M. Real-Time Probing of Electron Dynamics Using Attosecond Time-Resolved Spectroscopy. *Annu. Rev. Phys. Chem.* **67**, 41–63 (2016).
4. Mukamel, S., Healion, D., Zhang, Y. & Biggs, J. D. Multidimensional Attosecond Resonant X-Ray Spectroscopy of Molecules: Lessons from the Optical Regime. *Annu. Rev. Phys. Chem.* **64**, 101–127 (2013).
5. Ohmori, K. *et al.* Real-Time Observation of Phase-Controlled Molecular Wave-Packet Interference. *Phys. Rev. Lett.* **96**, 093002 (2006).
6. Weinacht, T. C., Ahn, J. & Bucksbaum, P. H. Measurement of the Amplitude and Phase of a Sculpted Rydberg Wave Packet. *Phys. Rev. Lett.* **80**, 5508–5511 (1998).
7. Childress, L. *et al.* Coherent Dynamics of Coupled Electron and Nuclear Spin Qubits in Diamond. *Science* **314**, 281–285 (2006).
8. Mukamel, S. *Principles of Nonlinear Optical Spectroscopy*. (Oxford University Press, 1999).
9. Cederbaum, L. S. Born–Oppenheimer approximation and beyond for time-dependent electronic processes. *J. Chem. Phys.* **128**, 124101 (2008).
10. Köuppel, H., Domcke, W. & Cederbaum, L. S. Multimode Molecular Dynamics Beyond the Born–Oppenheimer Approximation. in *Advances in Chemical Physics* 59–246 (John Wiley & Sons, Ltd, 1984). doi:10.1002/9780470142813.ch2
11. Geneaux Romain, Marroux Hugo J. B., Guggenmos Alexander, Neumark Daniel M. & Leone Stephen R. Transient absorption spectroscopy using high harmonic generation: a review of ultrafast X-ray dynamics in molecules and solids. *Philos. Trans. R. Soc. Math. Phys. Eng. Sci.* **377**, 20170463 (2019).



12. Okino, T. *et al.* Direct observation of an attosecond electron wave packet in a nitrogen molecule. *Sci. Adv.* **1**, e1500356 (2015).
13. Prince, K. C. *et al.* Coherent control with a short-wavelength free-electron laser. *Nat. Photonics* **10**, 176–179 (2016).
14. Goswami, D. Optical pulse shaping approaches to coherent control. *Phys. Rep.* **374**, 385–481 (2003).
15. Gauthier, D. *et al.* Spectrotemporal Shaping of Seeded Free-Electron Laser Pulses. *Phys. Rev. Lett.* **115**, (2015).
16. Sansone, G. *et al.* Shaping of attosecond pulses by phase-stabilized polarization gating. *Phys. Rev. A* **80**, 063837 (2009).
17. Allaria, E. *et al.* The FERMI free-electron lasers. *J. Synchrotron Radiat.* **22**, 485–491 (2015).
18. Gauthier, D. *et al.* Generation of Phase-Locked Pulses from a Seeded Free-Electron Laser. *Phys. Rev. Lett.* **116**, 024801 (2016).
19. Wituszek, A. *et al.* Stable interferometric platform for phase modulation of seeded free-electron lasers. *Opt. Lett.* **44**, 943–946 (2019).
20. Yu, L. H. Generation of intense UV radiation by subharmonically seeded single-pass free-electron lasers. *Phys. Rev. A* **44**, 5178 (1991).
21. Usenko, S. *et al.* Attosecond interferometry with self-amplified spontaneous emission of a free-electron laser. *Nat. Commun.* **8**, 15626 (2017).
22. Ribič, P. R. *et al.* Coherent soft X-ray pulses from an echo-enabled harmonic generation free-electron laser. *Nat. Photonics* **1** (2019). doi:10.1038/s41566-019-0427-1
23. Tan, H.-S. Theory and phase-cycling scheme selection principles of collinear phase coherent multi-dimensional optical spectroscopy. *J. Chem. Phys.* **129**, 124501 (2008).
24. Tian, P., Keusters, D., Suzuki, Y. & Warren, W. S. Femtosecond phase-coherent two-dimensional spectroscopy. *Science* **300**, 1553–1555 (2003).

25. Bruder, L. *et al.* Delocalized excitons and interaction effects in extremely dilute thermal ensembles. *Phys. Chem. Chem. Phys.* (2018). doi:10.1039/C8CP05851B
26. Hamm, P. & Zanni, M. *Concepts and Methods of 2D Infrared Spectroscopy*. (Cambridge University Press, 2011). doi:10.1017/CBO9780511675935
27. Ott, C. *et al.* Reconstruction and control of a time-dependent two-electron wave packet. *Nature* **516**, 374–378 (2014).
28. Warrick, E. R. *et al.* Multiple pulse coherent dynamics and wave packet control of the  $N_2 a''^1\Sigma+g$  dark state by attosecond four-wave mixing. *Faraday Discuss.* **212**, 157–174 (2018).
29. Fano, U. Effects of Configuration Interaction on Intensities and Phase Shifts. *Phys. Rev.* **124**, 1866–1878 (1961).
30. Madden, R. P., Ederer, D. L. & Codling, K. Resonances in the Photo-ionization Continuum of Ar  $i$  (20–150 eV). *Phys. Rev.* **177**, 136–151 (1969).
31. Wang, H. *et al.* Attosecond Time-Resolved Autoionization of Argon. *Phys. Rev. Lett.* **105**, (2010).
32. Trebino, R. *et al.* Measuring ultrashort laser pulses in the time-frequency domain using frequency-resolved optical gating. *Rev. Sci. Instrum.* **68**, 3277–3295 (1997).
33. Kowalewski, M., Bennett, K., Dorfman, K. E. & Mukamel, S. Catching Conical Intersections in the Act: Monitoring Transient Electronic Coherences by Attosecond Stimulated X-Ray Raman Signals. *Phys. Rev. Lett.* **115**, 193003 (2015).
34. Tekavec, P. F., Dyke, T. R. & Marcus, A. H. Wave packet interferometry and quantum state reconstruction by acousto-optic phase modulation. *J. Chem. Phys.* **125**, 194303 (2006).
35. Finetti, P. *et al.* Pulse Duration of Seeded Free-Electron Lasers. *Phys. Rev. X* **7**, (2017).
36. Bruder, L., Bangert, U. & Stienkemeier, F. Phase-modulated harmonic light spectroscopy. *Opt. Express* **25**, 5302 (2017).